

Solar Zenith Angle Variation of Clear-Sky Narrowband Albedos Derived from VIRS and
MODIS

Yan Chen, Sunny Sun-Mack, Qing Z. Trepte
SAIC, Hampton, VA, 23666

Patrick Minnis, David F. Young
NASA Langley Research Center, Hampton, VA

Abstract for the
11th AMS Conference on Atmospheric Radiation
Ogden, Utah
3 - 7 June 2002

P2.6 SOLAR ZENITH ANGLE VARIATION OF CLEAR-SKY NARROWBAND ALBEDOS DERIVED FROM VIRS AND MODIS

Yan Chen, Sunny Sun-Mack, Qing Z. Trepte
Science Applications International Corporation, Hampton, Virginia

Patrick Minnis*, David F. Young
Atmospheric Sciences, NASA Langley Research Center, Hampton, VA

1. INTRODUCTION

Satellite remote sensing of clouds using solar radiation requires an accurate estimate of the clear-sky reflectance for a given scene to differentiate cloudy from clear pixels. The clear-sky reflectance can be observed at one set of solar zenith (SZA), viewing zenith (VZA), and relative azimuth angles (RAA) for a limited set of conditions. To predict the clear-sky radiance at any other set of angles, it is necessary to know how the reflectance varies with the viewing and illumination angles. Typically, bidirectional reflectance distribution functions (BRDF) are used to predict the variation of reflectance with VZA and RAA for a given SZA. Directional reflectance models (DRM) describe the variation of albedo with SZA. The BRDFs are used to predict reflectance from albedo. DRMs depend on many factors, especially surface type. The accuracy of narrowband DRMs has traditionally been limited by uncertainties in the BRDF and biases in the sampling patterns from geostationary and sun-synchronous satellites. The Clouds and Earth's Radiant Energy System (CERES) project is using multispectral imagers, the 2-km resolution Visible Infrared Scanner (VIRS) on the Tropical Rainfall Measuring Mission (TRMM) satellite and the 1-km resolution Moderate Resolution Imaging Spectroradiometer (MODIS) on *Terra*, to detect clear and cloudy pixels and derive cloud properties. *TRMM*, launched during late 1997, continues to provide coverage at all local hours between 37°N and 37°S over a period of 46 days, while *Terra*, with MODIS operating since Spring 2000, has a 1030 LT Equatorial crossing time providing twice-per-day coverage in the Tropics and midlatitudes and higher temporal sampling in polar regions. A combination of the two datasets provides unprecedented angular sampling over all of the major surface types reducing the uncertainties associated with BRDFs and sampling patterns. This paper presents the results of an analysis of the clear-sky reflectances to determine the variation of 0.65 and 1.6- μm albedos with SZA and to examine the differences between the VIRS and MODIS spectral albedos.

*Corresponding author address: Patrick Minnis, NASA Langley Research Center, MS 420, Hampton, VA 23681-2199. email: p.minnis@larc.nasa.gov.

2. DATA AND ANALYSIS

Each MODIS and VIRS pixel is classified as either clear or cloudy using the latest update of the method described by Trepte et al. (1999). All clear pixels for a given overpass are averaged into the appropriate region defined by a 10' global grid. Each 10' region is assigned a single surface type K as defined by the International Geosphere Biosphere Programme (IGBP). The mean observed clear-sky reflectance for the overpass is

$$\rho_{\lambda} = \rho_{\lambda}(K; LAT, LON; \mu_o, \mu, \psi) \quad (1)$$

where λ is the wavelength, K is the International Geosphere Biosphere Programme (IGBP) surface type (see Table 1), LAT and LON are the latitude and longitude, respectively, μ_o and μ are the cosines of SZA and VZA, respectively, and ψ is RAZ. Instantaneous regional mean or pixel-level clear-sky reflectances comprise the fundamental data used here.

Clear-sky reflectance is a combination of radiation reflected by the atmosphere and the surface. For the VIS (0.65- μm) channels, the primary atmospheric effects are Rayleigh and aerosol scattering and ozone absorption, while water vapor absorption and aerosols are the primary attenuators in the near-infrared channel (NIR, 1.6 μm). Figure 1 shows the VIS and NIR filter functions for VIRS and MODIS. Differences in these filters for a given band suggest differences in atmospheric attenuation and perhaps surface reflectance. Calibration studies show that the VIRS VIS reflectance is up to 0.02 greater than MODIS at low reflectances (Minnis et al. 2002). Part of the difference is due to the spectral differences. Young et al. (2002) found that the VIRS NIR channel response is degrading at $\sim 3.4\%$ /year.

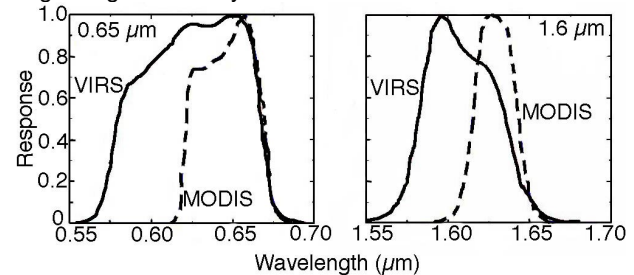


Fig. 1. Filter functions for VIRS and MODIS.

K	IGBP type
1	evergreen needle leaf
2	evergreen broadleaf
3	deciduous needle leaf
4	deciduous broadleaf
5	mixed forest (conifer + broadleaf)
6	closed shrubland
7	open shrubland
8	woody savanna
9	savanna
10	grassland
11	permanent wetlands
12	croplands
13	urban
14	mixed grass-forest
15	snow/ice
16	desert, barren/sparse vegetation
17	water
18	tundra
19	coastline (10 to 90% water)

2.1 VIS clear-sky albedos

The top-of-the-atmosphere VIS albedo is

$$\alpha_{VIS} = \rho_{VIS}(K; LAT, LON; \mu_o, \mu, \psi) / \chi_{VIS}(K; \mu_o, \mu, \psi), \quad (2)$$

where the VIS BRDFs are taken from Minnis and Harrison (1984) for water and from Suttles et al. (1988) for land ($K = 1-14, 18$), snow, and desert. The observed pixel-level reflectances were converted to TOA albedos and averaged for a given $10'$ region. Two datasets were developed from these albedos. An overhead-sun ($\mu_o = 1$) albedo $\alpha_{VIS}(K, 1)$ dataset was derived by adjusting the observed albedo to $\mu_o = 1$ using the normalized DRMs developed by Sun-Mack et al. (1999). The results for a given region were averaged for the month to provide a monthly mean clear-sky albedo for each region. Surface type average overhead-sun albedos were also computed for each month using the individual regional results. Instantaneous regional albedos were also averaged according to surface type and μ_o bin defined for each 0.1 increment of μ_o between 0 and 1. This latter dataset is used to study the SZA dependence of albedo.

2.1 NIR surface albedos

Neglecting aerosols, the observed NIR reflectance can be approximated as,

$$\rho_{NIR} = \alpha_{SNIR} \chi_{NIR}(K; \mu_o, \mu, \psi) t_{NIR}, \quad (3)$$

where α_{SNIR} is the surface albedo and χ_{NIR} is the normalized BRDF for the surface, and t_{NIR} is the combined transmittance of the atmosphere to the downwelling solar beam and upwelling diffuse radiation. It is estimated as

$$t_{NIR} = \exp[-\tau_{NIR}(1/\mu_o + 2.04)], \quad (4)$$

where τ_{NIR} is the water vapor optical depth parameterized as a function of the precipitable water, surface pressure,

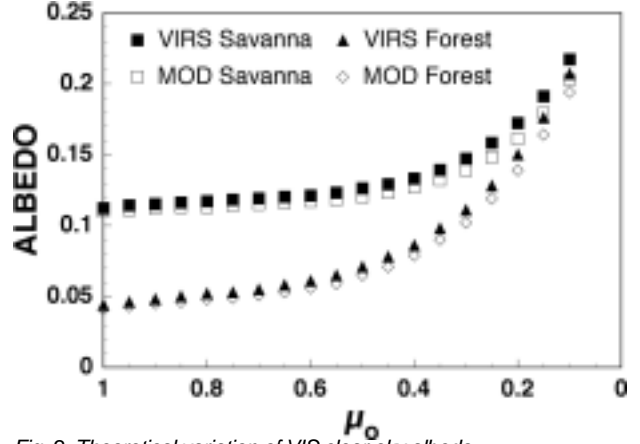


Fig. 2. Theoretical variation of VIS clear-sky albedo.

μ_o , and LAT based on results of detailed radiative transfer calculations using correlated k-distribution calculations for the VIRS NIR channel following Kratz (1995).

The NIR BRDFs for most surface types were derived from the aircraft measurements of Kriebel (1978) taken at $1.66 \mu m$ for four distinct surfaces. The coniferous forest model was used for all forest types ($K = 1, 5$), while bog was used for $K = 11, 18$, and 19 . The savanna data were used for $K = 6, 7, 8, 9$, and 13 and the pasture results were used for $K = 10, 12$, and 14 . The updated VIS ocean model from Minnis and Harrison (1984) was used for water, while the snow and desert models from Suttles et al. (1988) were used for $K = 15$ and 16 , respectively.

3. RESULTS

Figure 2 shows the variation of clear-sky VIS top-of-atmosphere (TOA) albedo computed using the surface albedos derived from the Kriebel (1978) data using an adding-doubling radiative transfer model with nominal ozone absorption and Rayleigh scattering derived using the filter functions in Fig. 1. The savanna clear-sky albedos are nearly 3 times greater than the forest albedos for $\mu_o = 1$, but are nearly equal for $\mu_o = 0.1$. All albedos computed using the MODIS Rayleigh scattering are smaller than the corresponding VIRS albedos. For these relatively dark scenes, the VIRS albedo should be 2 - 10% greater than the MODIS albedos depending on the SZA and surface type.

An examination of the overhead sun albedos derived from VIRS and MODIS during April 2001 reveals that the MODIS albedos are nearly always smaller than the VIRS albedos by 0.01 to 0.03 for heavily vegetated surfaces, where the TOA VIS albedos are 0.2 or less. However, for clear deserts and shrublands, the MODIS VIS albedos were 0.01 to 0.06 larger than the VIRS albedos. For the larger albedos, the Rayleigh scattering and absorption have less impact on the MODIS radiances while suppressing the VIRS albedos. Small spectral differences in the surface reflectances can also affect the TOA albedo differences. The MODIS ocean albedos

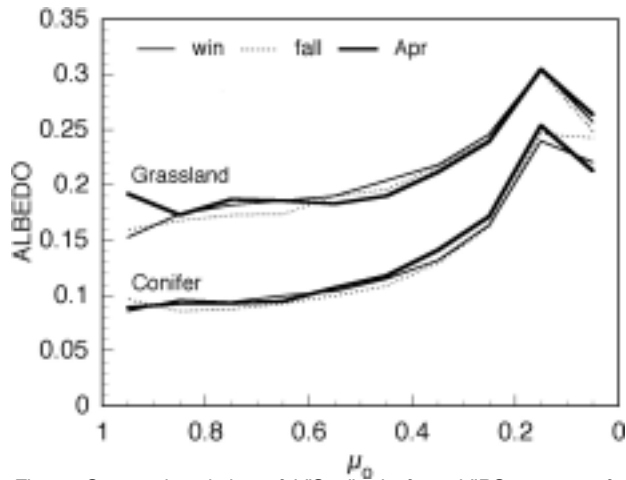


Fig. 3. Seasonal variation of VIS albedo from VIRS 1998-99 for conifer forest and grassland.

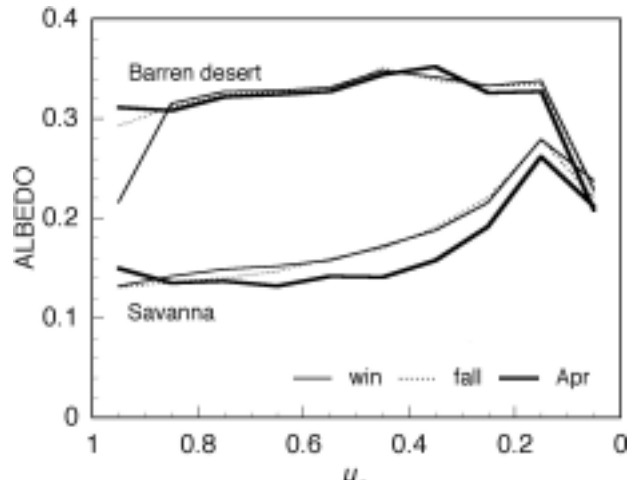


Fig. 6. Same as Fig. 3, except for desert and savanna.

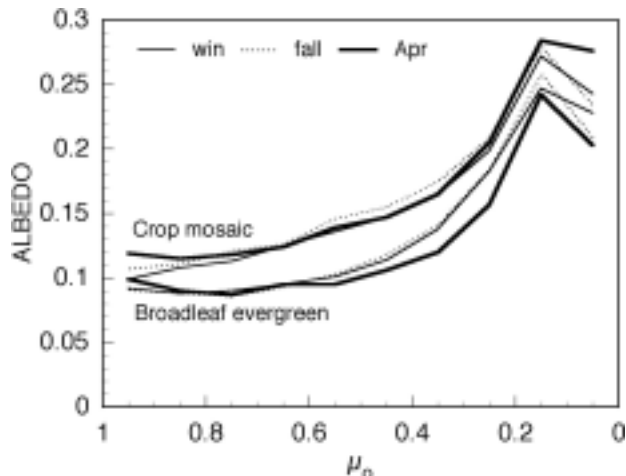


Fig. 4. Same as Fig. 3, except for crop-mosaic and broadleaf evergreen forests.

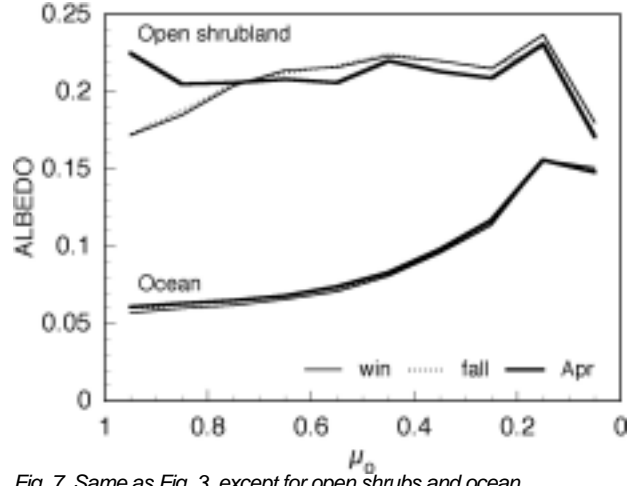


Fig. 7. Same as Fig. 3, except for open shrubs and ocean.

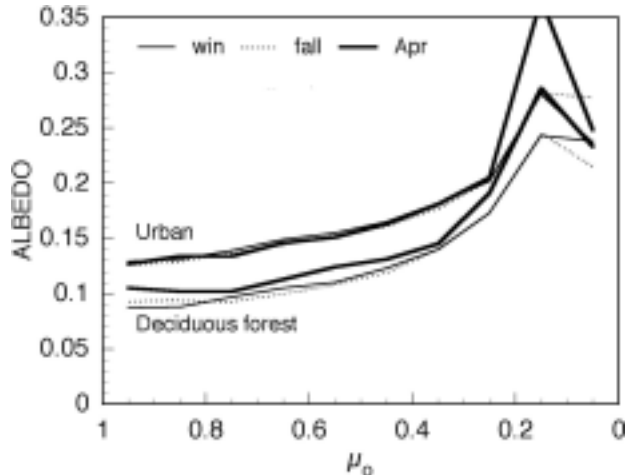


Fig. 4. Same as Fig. 3, except for deciduous forests and urban.

average almost 0.01 less than the VIRS albedos indicating that the CERES cloud analysis code needs to reduce the overhead sun albedos used of detecting and analyzing clouds over water surfaces.

The clear-sky albedos derived from VIRS data taken during boreal autumn and winter 1998-99 and during April 2001 are plotted in Figs. 3 - 7 for a variety of surface types. The decrease in albedo for $\mu_0 < 0.15$ is an artifact that should be ignored in all cases. The variation of albedo for $\mu_0 = 0.95$ is likely to be the result of sampling variations with seasons and should be considered suspect. All of the forest albedos are less than those for the other surface types. The forest and crop-mosaic albedos increase by a factor 3 over the SZA range while the savanna, urban, and grassland albedos only increase by a factor of 2. The desert (Fig. 6) and shrubland (Fig. 7) albedos vary minimally with SZA. The SZA variation of conifer forest and urban albedos is seasonally consistent whereas the deciduous forest albedos are slightly variable with maximum values occurring during April. The crop-mosaic albedos peak during the fall when the deciduous forest and grassland values are at their lowest. The ocean albedos change very little with season also. The SZA changes in the savanna and conifer forest albedos closely resemble those in Fig. 2 except that the magnitudes are larger. The surface albedos were measured using a narrow spectral

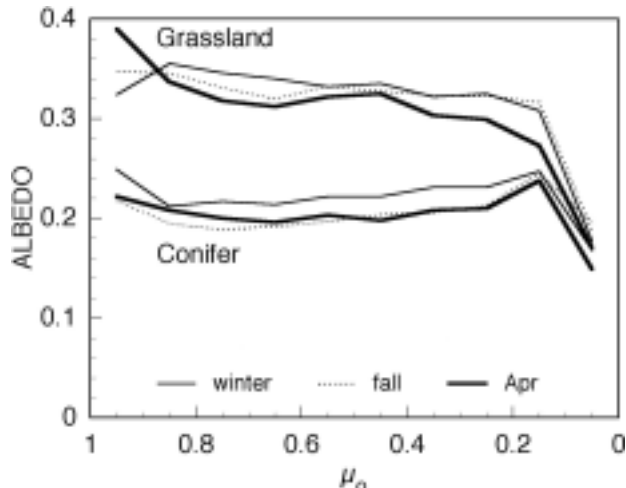


Fig. 8. Seasonal variation of NIR albedo from VIRS 1998-99 for conifer forest and grassland.

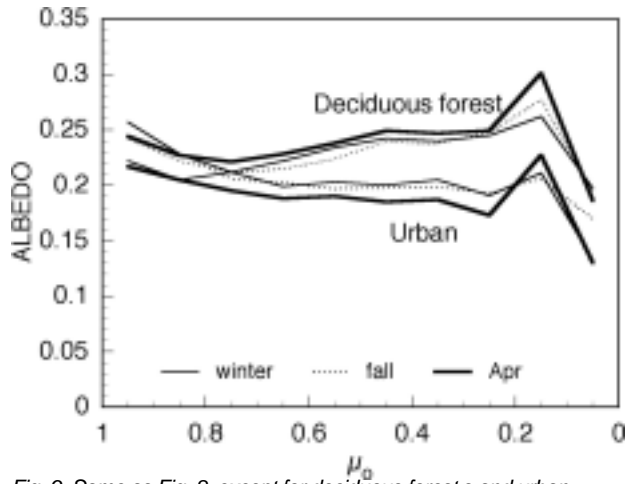


Fig. 9. Same as Fig. 8, except for deciduous forests and urban.

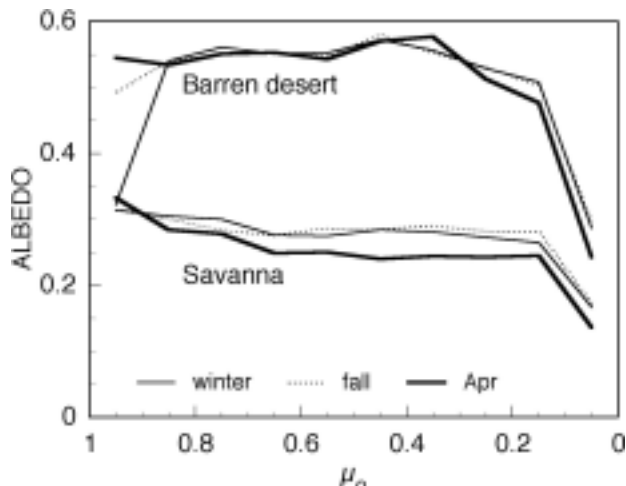


Fig. 10. Same as Fig. 8, except for desert and savanna.

filter and the TOA albedos were measured with the broad VIRS filter (Fig. 1) that includes the green reflectance peak. Additionally, the observed albedos include aerosol scattering, which will increase the TOA albedo.

Examples of the albedo variations with SZA for the VIRS NIR channel are plotted in Figs. 8 - 10. In all cases, except for the deciduous forest and urban (Fig. 9), the NIR albedos for each pair of surface types differ by the same sign as their VIS counterparts. Overall, the NIR albedos are relatively constant with SZA for nearly all surfaces. The forest albedos all exhibit a slight tendency to increase with SZA while albedos for the remaining surface types tend to decrease with SZA if they vary at all. The ocean NIR albedos (not shown) are ~ 0.025 at overhead sun and increase to 0.05 at $\mu_0 = 0.15$. Except for ocean and snow, the NIR albedos are markedly greater than their VIS counterparts.

4. CONCLUDING REMARKS

The results discussed here from indicate that the VIS albedos from MODIS and VIRS are significantly different and should be determined separately for each sensor. The CERES system updates the clear-sky albedos for land but requires an explicit correction for the ocean albedo. These results will be used to develop refined DRMs that will be used to better predict clear-sky reflectance at the VIS and NIR wavelengths.

5. REFERENCES

- Kratz, D. P., 1995: The correlated k-distribution technique as applied to the AVHRR channels. *J. Quant. Spectrosc. Radiat. Transfer*, **53**, 501-507.
- Kriebel, K. T., 1978: Measured spectral bidirectional reflectance properties of vegetated surfaces. *Appl. Opt.*, **17**, 253-259.
- Minnis, P. and E. F. Harrison, 1984: Diurnal variability of regional cloud and clear-sky radiative parameters derived from GOES data. Part III: November 1978 radiative parameters. *J. Climate Appl. Meteor.*, **23**, 1032-1051.
- Minnis, P., L. Nguyen, D. R. Doelling, D. F. Young, W. F. Miller, and D. P. Kratz, 2002: Rapid calibration of operational and research meteorological satellite imagers. Part I and II. *J. Atmos. Oceanic Technol.*, in press.
- Sun-Mack, S., Y. Chen, T. D. Murray, P. Minnis, and D. F. Young, 1999: Visible clear-sky and near-infrared surface albedos derived from VIRS for CERES. *Proc. AMS 10th Conf. Atmos. Rad.*, Madison, WI, June 28 - July 2, 422-425.
- Suttles, J. T., R. N. Green, P. Minnis, G. L. Smith, W. F. Staylor, B. A. Wielicki, I. Walker, D. F. Young, V. R. Taylor, and L. L. Stowe, 1988: Angular radiation models for Earth-atmosphere system, Vol. 1, Shortwave radiation. *NASA RP-1184*, 144 pp.
- Trepte, Q., et al., 1999: Scene identification for the CERES cloud analysis subsystem. *Proc. AMS 10th Conf. Atmos. Rad.*, 28 June - 2 July, Madison, WI.
- Young, D. F., P. Minnis, and L. Nguyen, 2001: Evaluation of the TRMM 1.6- μm channel calibration. Submitted to *J. Atmos. Oceanic Technol.*